ISSN 0915-633X

NATIONAL INSTITUTE FOR FUSION SCIENCE

Edge Plasma Density Reconstruction for Fast Monoenergetic Lithium Beam Probing

S. Sasaki, S. Takamura, M. Ueda, H. Iguchi, J. Fujita and K. Kadota

(Received – Apr. 13, 1992)

NIFS-147 May 1992

RESEARCH REPORT
NIFS Series

NAGOYA, JAPAN

"Edge Plasma Density Reconstruction for Fast Monoenergetic Lithium Beam Probing"

S. Sasaki, S. Takamura

Department of Electrical Engineering and Electronics, Faculty of Engineering, Nagoya University, Nagoya, 464-01, Japan

M. Ueda [a], **H. Iguchi, J. Fujita**

National Institute for Fusion Science, Nagoya, 464-01, Japan

K. Kadota

Plasma Science Center, Nagoya University, Nagoya 464-01, Japan

ABSTRACT

Two types of plasma density reconstruction methods for fast Li^0 beam probe diagnostics have been developed for edge profile measurements in the CHS helical device, in which density dependence of atomic processes such as ionization, excitation/ deexcitation and charge exchange is introduced by the use of effective rate coefficients calculated from collisional radiative model. These methods enable us to get plasma density profile well inside the last closed flux surface (LCFS) for various range of plasma densities with considering attenuation of the fast Li^0 beam and using effective rate coefficients. A new method (method-I) can unfold the plasma density profiles from a fractional part of emission profile of Li I resonance line. The second method (method-II) reconstructs the density profile from the whole range of emission profile including signal tail-off region due to the beam attenuation. These two methods, which introduce density dependence of atomic processes and the beam attenuation caused by ionization, noticeably improve the precision of the measurements and extend the applicable density region of the plasma. Density profiles reconstructed by these two different methods have shown good agreement each other and are consistent with the result of ruby laser Thomson scattering.

Keywords: density reconstruction , fast neutral lithium beam probing, multi step atomic processes, CHS edge plasma

---

[a] Permanent address: Instituto Nacional de Pesquisas Espaciais, São José dos Campos, São Paulo, 12201, Brazil

I. INTRODUCTION

The determination of plasma parameters at the edge region of fusion devices has deserved much attention with respect to generation and transport of impurities and to improvement of global confinement of fusion plasmas. Beam Emission Spectroscopy (BES) using three types of neutral lithium atomic beam, namely, thermal beam [1-3], laser blow-off beam [1,4-8] and fast beam [1,9-12] are now considered to be one of the most powerful techniques to determine the edge plasma density profile without perturbation nor contamination to the confined plasmas. Plasma density profile is directly obtained or reconstructed from Li I resonance line (6708Å) emission signal from the injected Li^0 atoms excited by electron or proton impact with the aid of atomic data of excitation, ionization and charge exchange processes.

Three types of Li^0 beams have different characteristics in the velocity distribution. How deep in the plasma the method is applicable depends on the penetration length l_p of the beam. It is often evaluated by the product of line averaged plasma density $\bar{n}$ and l_p. A thermal beam whose mean velocity is of the order of 10^5 cm/s is applicable to plasmas up to $\bar{n} \times l_p$ of 10^{12} cm^{-2}. Hence the penetration length of thermal beam is only several centimeters even for the edge plasma with denstiy below 10^{12} cm^{-3}. Because of slow beam velocity and low density and temperature of the target plasma in this case, electron impact excitation and ionization are dominant processes, and the electron impact processes of excited Li^0 is negligible. Plasma density profiles have been obtained using thermal beams in TEXTOR tokamak [1], CASTOR tokamak [2] and Heliotron-E helical device [3]. Plasma density is reconstructed taking the velocity distribution of the thermal beam into account in the case of CASTOR and Heliotron-E. A laser blow-off beam whose mean velocity is of the order of 10^6 cm/s is applicable to plasmas up to $\bar{n} \times lp$ of 10^{13} cm^{-2}. Electron impact processes are still dominant. Because of relatively high density of the target plasma ($\geq 10^{12}$ cm^{-3}), ionization and deexcitation processes from Li^0 excited states make an increase of ionization probability and a decrease of emission probability. Density dependence of ionization and emission processes is obtained using effective rate coefficients calculated from collisional radiative model in the density profile reconstruction in the HYBTOK-II tokamak[6,7]. Effects of transient characteristic of the laser blow-off beam are also successfully resolved by the use of high speed shuttering of emission profile (~10μs) and reconstruction considering

the transport of laser blow-off Li^0 beam. A monoenergetic fast Li^0 beam with energy above several keV has $\bar{n} \times l_p$ above 10^{14} cm^{-2} and can penetrate more than several tens centimeters into the plasma with density above 10^{13} cm^{-3}. BES using a fast Li^0 beam has been applied in a bumpy torus NBT (4 keV) [10,11] and in tokamaks like TEXTOR (20keV~30keV) [1] and ASDEX (40~100 keV) [12]. In the case of fast beam, proton impact processes for the excitation, deexcitation, ionization and charge exchange as well as electron impact processes must be considered.

In this paper two methods of density reconstruction using a fast Li^0 beam are described for the measurements of edge density profile in CHS [13]. Beam energy of 8 keV is selected to satisfy two conditions conflicting each other; penetration length and spatial resolution. The fast Li^0 beam with energy of 8 keV, whose $\bar{n} \times l_p$ is 2.6×10^{14} cm^{-2}, can penetrate inside the last closed flux surface (LCFS) of the CHS plasma. Spatial resolution of 1.3cm, which is determined by the product of the beam velocity and lifetime of Li^0 excited state, is sufficient for the edge density profile measurement. To obtain edge density profile, two problems must be solved; density dependence of atomic processes and attenuation of the beam. In the past experiments of density measurements by BES in NBT [10,11], a calibration of beam intensity and optical system using hydrogen molecule impact excitation was adopted and these problems, which may cause errors in high density region above 5×10^{12} cm^{-3}, depending on the density profile, were neglected (simple BES measurement). A new density reconstruction method (method-I) solves these problems by using effective rate coefficients including the effects of proton impact and beam attenuation caused by ionization. This new method considerably extends the accessible density range compared to the simple BES measurement. We also make the density reconstruction method from the whole range of emission profile (method-II) by the use of the effective rate coefficients, which can be applied to higher density plasmas. By selecting these two types of reconstruction methods, density profiles under various discharge conditions can be obtained.

II. EXPERIMENTAL APPARATUS

Experimental set up of the fast Li^0 beam probing system on the CHS helical device is shown in Fig.1 [14,15]. CHS is a heliotron/torsatron type device which has a major radius of 100cm; a minor radius of the helical field coil of 31cm; the pole number and the toroidal

period number of the helical field coil of l=2 and m=8, respectively. A hydrogen plasma is produced by electron cyclotron resonance (ECR) heating with the frequency of 53GHz and the power of 150kW. A 45keV neutral beam injector with the power up to 1MW is utilized for the additional heating. A fast Li^0 beam for BES is supplied by a monoenergetic and continuous neutral beam source. Li^+ ions extracted from the ion gun which consists of an ion source of thermionic emission type (ß-eucryptite), a Pierce extracter and cylindrical lens are neutralized by charge exchange as they pass through a cell containing Cs vapor [11]. Extracted Li^0 beam has an equivalent beam current density of 50μA/cm^2 at 8keV, and a diameter of 15-20mm in FWHM at the diagnostics position. Li I resonance line (6708Å) emitted from excited Li^0 atoms is detected by a photomultiplier tube through lens, fiber optics and an interference filter with FWHM of 15Å. In order to improve the signal to noise ratio, the Li^0 beam is modulated at 10kHz and phase sensitive detection is used. Since we have only a single channel detector at the moment, spatial emission profile is obtained by changing the point of observation in a series of identical discharges. In the present set-up, observable position is restricted to x~113-126cm in major radius, that is, outside edge of the toroidal plasma. The detail of the experimental procedure will be described in elsewhere [15].

III. DENSITY DEPENDENCE OF LITHIUM EMISSION AND IONIZATION PROCESSES

Because of the finite life time of Li I excited state 2^2P (27ns) and relatively high plasma density in the CHS edge region, atomic processes are not simple. In addition to the basic transition processes connected with the ground state 2^2S, transitions from the excited state 2^2P induced by electron and proton impact should be evaluated. Then the ionization and emission rates depend on the local plasma density. Those transition processes and their rate coefficients among ground state, excited state and ionized state are summarized in Fig.2. Rate coefficients are calculated assuming plasma temperature of 30 eV and the beam energy of 8 keV. The recombination process can be neglected since the diffusion process of Li^+ ion along magnetic field is much faster than that of recombination. Higher excited states are also neglected since their population is much smaller than that of 2^2P state.

Rate coefficients for each process are evaluated from the atomic data experimentally or empirically obtained. Ionization from 2^2S, ionization from 2^2P, excitation from 2^2S to 2^2P and its deexcitation in electron impact processes are expressed by $\langle\sigma_{is}v_e\rangle$, $\langle\sigma_{ip}v_e\rangle$, $\langle\sigma_{ex}v_e\rangle$ and $\langle\sigma_{dex}v_e\rangle$, respectively [4,6,16]. Since electron thermal motion with temperature of 30eV is much faster than 8 keV Li^0 beam, rate coefficients for electron impact processes are calculated neglecting the velocity of Li^0 beam. Since these rate coefficients have so weak dependence on electron temperature in the range of 10-100eV that they can be treated as constants. Corresponding proton impact processes are expressed as $\langle\sigma_{is}v_p\rangle$, $\langle\sigma_{ip}v_p\rangle$, $\langle\sigma_{ex}v_p\rangle$ and $\langle\sigma_{dex}v_p\rangle$. These rate coefficients are calculated based on the data in the reference [16]. Charge exchange of Li^0 atom with plasma proton is also important, and its rate coefficients for 2^2S and 2^2P states are expressed as $\langle\sigma_{cs}v_p\rangle$ and $\langle\sigma_{cp}v_p\rangle$ respectively. In this case the thermal motion of plasma proton with temperature of 30eV can be neglected. From the same reason, rate coefficients for the proton impact processes have so weak dependence on the plasma temperature. Since there is no data of charge exchange cross section for excited $Li^0(2^2P)$ atom σ_{cp}, it is estimated from the cross section for $Cs^0(5^2S)$ because these two states have a similar electron structure in outermost electron orbit and similar energy difference ΔE before and after the charge exchange reaction as follows: [16,17]

$$Cs^0(5^2S) + H^+ \rightarrow Cs^+ + H^0 + \Delta E\ . \qquad \cdots\cdots (1)$$

Here we introduce total rate coefficient for ionization $\langle\sigma_{is}v\rangle$ for 2^2S state as

$$n\langle\sigma_{is}v\rangle n_{Li} = n(\langle\sigma_{is}v_e\rangle + \langle\sigma_{is}v_p\rangle + \langle\sigma_{cs}v_p\rangle)\, n_{Li}\ , \qquad \cdots\cdots (2)$$

where n and n_{Li} is the plasma density and density of fast Li^0 beam, respectively, and $Z_{eff}=1$ is assumed, i.e. the proton density is equal to the electron density. In the similar way total rate coefficients for other processes are defined. They are summerized as follows with the values for the edge plasma parameters mentioned above.

$$\langle\sigma_{is}v\rangle = \langle\sigma_{is}v_e\rangle + \langle\sigma_{is}v_p\rangle + \langle\sigma_{cs}v_p\rangle = 1.8\times10^{-7}\ cm^3/s\ ,$$

$$\langle\sigma_{ip}v\rangle = \langle\sigma_{ip}v_e\rangle + \langle\sigma_{ip}v_p\rangle + \langle\sigma_{cp}v_p\rangle = 7.3\times10^{-7}\ cm^3/s\ ,$$

$$\langle\sigma_{ex}v\rangle = \langle\sigma_{ex}v_e\rangle + \langle\sigma_{ex}v_p\rangle = 8.9\times10^{-7}\ cm^3/s\ ,$$

$$\langle\sigma_{dex}v\rangle = \langle\sigma_{dex}v_e\rangle + \langle\sigma_{dex}v_p\rangle = 2.8\times10^{-7}\ \mathrm{cm^3/s}\,. \qquad \cdots\cdots (3)$$

Then effective rate coefficients for ionization and emission of Li^0 atom are expressed in terms of these total rate coefficients. In the collisional radiative model, rate equation expressed as following equation is assumed to be zero.

$$\frac{dn_{Li}^*}{dt} = n\langle\sigma_{ex}v\rangle n_{Li} - n\langle\sigma_{ip}v\rangle n_{Li}^* - n\langle\sigma_{dex}v\rangle n_{Li}^* - \frac{n_{Li}^*}{\tau_{em}} = 0\,, \qquad \cdots\cdots (4)$$

where n_{Li}, n_{Li}^* and τ_{em} are the density of neutral lithium atoms which is approximately equal to that of ground state, that of excited state and the life time of Li^0 excited state (27ns), respectively. Modifying eq.(4), n_{Li}^* can be expressed as a function of n_{Li} and n.

$$n_{Li}^* = \frac{\langle\sigma_{ex}v\rangle \tau_{em}\, n}{1+\left(\langle\sigma_{ip}v\rangle + \langle\sigma_{dex}v\rangle\right)\tau_{em}\, n}\, n_{Li}\,. \qquad \cdots\cdots (5)$$

Ionization rate is expressed by using effective ionization rate coefficient $\langle\sigma_i v\rangle_{eff}$.

$$\frac{dn_{Li^+}}{dt} = n\langle\sigma_i v\rangle_{eff}\, n_{Li}\,. \qquad \cdots\cdots (6)$$

In our case, density of neutral Emission photon flux N_{vp} to the detector is expressed by using effective emission rate coefficient $\langle\sigma_{em}v\rangle_{eff}$.

$$N_{vp} = n\langle\sigma_{em}v\rangle_{eff}\, n_{Li}\, V\frac{\Omega}{4\pi}\,, \qquad \cdots\cdots (7)$$

where V and Ω mean the observation volume [cm^3], the solid angle of the optical detection system [str], respectively. From eqs.(5), (6) and (7), effective ionization and emission rate coefficients are expressed as,

$$\frac{\langle\sigma_i v\rangle_{eff}}{\langle\sigma_{is}v\rangle} = 1 + \frac{\langle\sigma_{ip}v\rangle\langle\sigma_{ex}v\rangle\tau_{em}\, n}{\langle\sigma_{is}v\rangle\left(1+\left(\langle\sigma_{ip}v\rangle + \langle\sigma_{dex}v\rangle\right)\tau_{em}\, n\right)}\,,$$

$$\frac{\langle\sigma_{em}v\rangle_{eff}}{\langle\sigma_{ex}v\rangle} = \frac{1}{1+\left(\langle\sigma_{ip}v\rangle + \langle\sigma_{dex}v\rangle\right)\tau_{em}\, n}\,. \qquad \cdots\cdots (8)$$

It is clear from eq.(8) that the effective rate coefficient is density dependent because of finite life time τ_{em} and non-negligible effect of ionization and deexcitation from 2^2P state.

The dependence is shown in Fig.3. An increase of ionization rate and decrease of emission rate due to an increase of population of 2^2P state are pronounced when the plasma density is above 10^{12} cm^{-3}. As much as 75% increase of ionization rate and 29% decrease of emission rate can be seen in Fig.3, when the plasma density reaches up to 10^{13} cm^{-3}. Penetration length of 8 keV Li^0 beam in the plasma with density of 1×10^{13} cm^{-3} is estimated to be 14.9 cm by using effective ionization rate coefficient. Under this condition, as much as 29 % of the beam is lost in the path length of 5cm. Both the beam attenuation and the decrease of emission rate coefficient influence on the BES measurements.

A contribution from higher excited states of Li^0 atom could also exist at much higher density region. This modeling is suitable for the density measurement below 5×10^{13} cm^{-3}. The high density effects are simply introduced by the use of effective rate coefficients defined by eqs.(8).

IV. METHOD OF DENSITY RECONSTRUCTION WITH THE AID OF GAS CALIBRATION (METHOD-I)

A. Determination of local density by simple BES measurement

In the simple BES measurement using the fast Li^0 beam, determination of local electron density is performed through calibration of beam intensity and optical detection system by the use of gas atom impact excitation, which is similar to calibration of laser system in Thomson scattering. Helium gas at the pressure range of the order of 10^{-4} Torr are used as a target gas in the CHS. In this pressure range beam attenuation is negligible. Signal output I_g [V] from the Li^0 atoms excited by the impact with calibration gas atom can be written as,

$$I_g(x) = n_g \, \sigma_{ex\text{-}g} \, v_{Li} \, n_{Li}(x) \, V \frac{\Omega}{4\pi} \eta \,, \qquad \cdots\cdots (9)$$

where n_g, $\sigma_{ex\text{-}g}$, v_{Li}, and η are the density of He gas [cm^{-3}], the excitation cross section of Li^0 atom by the collision with He atom [cm^2], the beam velocity [cm/s] and the sensitivity of the optical detection system [V·s/photon], respectively. We introduce inverse sensitivity of the beam probe system w_0 as

$$w_0 = \frac{1}{n_{Li} V \frac{\Omega}{4\pi} \eta} = \frac{n_g \sigma_{ex\text{-}g} v_{Li}}{I_g}, \quad \cdots\cdots (10)$$

which can be obtained from the measured value of n_g and I_g in the calibration work. In the present case, w_0 is 2.4×10^6 $[V^{-1}\cdot s^{-1}]$.

Signal output $I_{Li}(x)$ from the excited Li^0 atom in the plasma at the position x is expressed as follows using effective emission rate coefficient.

$$I_{Li}(x) = n(x) \langle \sigma_{em} v \rangle_{eff} n_{Li}(x) V \frac{\Omega}{4\pi} \eta, \quad \cdots\cdots (11)$$

where n(x) is the local plasma density and x is the observation position in major radius [cm]. From eqs.(10) and (11) the plasma density can be determined by,

$$n(x) = \frac{I_{Li}(x)}{\langle \sigma_{em} v \rangle_{eff}} w_0 = \frac{I_{Li}(x)}{I_g} \frac{\sigma_{ex\text{-}g} v_{Li}}{\langle \sigma_{em} v \rangle_{eff}} n_g . \quad \cdots\cdots (12)$$

Since we know the value of w_0, the local density is determined from the relative intensity ratio $I_{Li}(x)/I_g$. This is correct only in the case that the beam attenuation is negligibly small. This simple density determination method was successfully applied to a relatively low density plasma in the CHS [15] as well as NBT [10,11]. Plasma densities measured by the simple BES at 60 ms in the discharge sequence when the plasma is sustained by ECR at toroidal magnetic field of 0.89 T are shown by crossess in Fig.4. Vacuum magnetic axis and last closed flux surface (LCFS) crossing the Li^0 beam path are at 92.1 cm and 119.0 cm, respectively. Electron densities measured by Thomson scattering on the same magnetic flux surface but 67.5° separated in toroidal direction are shown by dots with error bars.

[B]Density reconstruction considering beam attenuation

In order to evaluate effects of beam attenuation and density dependence of the emission rate coefficient, a numerical simulation is carried out. Here we assumed a parabolic plasma density profile with the edge value of 1×10^{12} cm^{-3} and central value of 3×10^{13} cm^{-3} and the plasma radius of 20cm. In the simulation, y-coordinate means the distance from the edge toward the center. In Fig.5(a), beam density (thick-dashed curve) is calculated by eq.(13) shown later and the emission signal (thin-dotted one) is calculated by eq.(11)

considering beam attenuation. The plasma density determined by simple BES simulation from eq.(12) putting $\langle\sigma_{em}v\rangle_{eff} = \langle\sigma_{ex}v\rangle$ is also shown (thick-solid one). It should be noted that beam attenuation is so strong that error in density determination reaches up to -45% at the position where emission profile has a peak (z=5.2cm). Density reconstruction error depends on both the effects of beam attenuation and the decrease of effective emission rate coefficients in the higher density region. The accessible region for simple BES measurement depends on the edge density profile. In CHS plasma, it was found that the density distribution is near exponential one rather than parabolic one, which gives larger penetration length as shown in Fig.4.

A new density reconstruction method, classified as method-I, is developed to solve these problems. The attenuation of monoenergetic Li^0 beam with the velocity of v_{Li} is expressed by,

$$\frac{n_{Li}(z)}{n_{Li}(0)} = \exp\left[-\int_0^z \frac{\langle\sigma_i v\rangle_{eff}}{v_{Li}} n(\zeta)\, d\zeta\right], \qquad \cdots\cdots (13)$$

where we introduce a new coordinate z, which means the distance from the plasma edge toward smaller major radius. By the use of eqs.(10) and (13), eq.(11) is modified to

$$I_{Li}^{\dagger}(z) = \frac{n(z)\langle\sigma_{em}v\rangle_{eff}}{w_0} \exp\left[-\int_0^z \frac{\langle\sigma_i v\rangle_{eff}}{v_{Li}} n(\zeta)\, d\zeta\right]. \qquad \cdots\cdots (14)$$

Plasma density can be calculated iteratively from the edge toward the center. The density at the point z is determined so that the observed emission signal $I_{Li}(z)$ coincides with $I_{Li}^{\dagger}(z)$ which is re-calculated by eq.(14). For the iterative calculations, plasma density profile calculated from eq.(12) putting $\langle\sigma_{em}v\rangle_{eff} = \langle\sigma_{ex}v\rangle$ is used as the initial plasma density. Convergence speed and precision of the calculation can be optimized by the use of an appropriate convergence factor $f(I_{Li}(z)-I_{Li}^{\dagger}(z))$. Errors in density reconstruction depend not only on the measurement of $I_{Li}(z)$ but also on the accuracy of the atomic data and on the calibration procedure.

Reconstructed plasma density profile in the simulation is shown in Fig.5(b). It should be noted that accuracy of this method greatly depends on the accuracy of the

calibration for w_0. Density profile reconstructed using correct w_0, i.e. the same w_0 used in calculation of emission signal, is shown (thick-solid curve) in the figure. Two incorrectly reconstructed curves are obtained assuming 10% overestimate (thick-dotted one) or 10% underestimate (thick-dashed one) of w_0. Errors in the density at the position where the emission profile has a peak reach up to -18% and +30%, respectively.

An example of density profile measurement in the typical CHS discharge is shown in Fig.6. The plasma is sustained by NBI at toroidal magnetic field of 1T. The magnetic axis is set at the major radius of 94.9 cm and the position of the last closed flux surface (LCFS) is 122.5 cm. Emission signal at 80 ms in the discharge sequence (thin-dotted curve) is spline interpolated since this method needs emission profile to calculate the beam attenuation. By the use of this reconstruction method-I, we can obtain the density profile (thick-solid curve) with the help of the simple BES measurement putting $\langle\sigma_{em}v\rangle_{eff} = \langle\sigma_{ex}v\rangle$ as shown in thin-solid one. Effects for uncertainty of atomic data are relatively small compared with the reconstruction method-II which will be described in the next section, because the plasma density near the edge where the beam attenuation and the density dependence of atomic processes are neglected is almost determined by simple BES measurement. The fact that density profile can be reconstructed from the fractional part of the emission profile near the edge is an advantage of this method-I.

V. METHOD OF DENSITY RECONSTRUCTION FROM THE WHOLE EMISSION PROFILE (METHOD-II)

The second density reconstruction method, classified as method-II, requires the whole region of the emission profile from the edge of the plasma to the region where the emission signal is totally attenuated. Since the ratio of probability of ionization to that of emission is proportional to $\langle\sigma_i v\rangle_{eff}/\langle\sigma_{em}v\rangle_{eff}$, the Li^0 beam density can be calculated from following equation [5],

$$n_{Li}(x) = \frac{\displaystyle\int_0^x \frac{\langle\sigma_i v\rangle_{eff}}{\langle\sigma_{em}v\rangle_{eff}} I_{Li}(\xi)\, d\xi}{v_{Li}\, V \frac{\Omega}{4\pi}\eta}. \qquad \cdots\cdots (15)$$

Note that $n_{Li}(x)$ is integrated from the position of interior plasma where the beam is totally

attenuated to outward direction from which Li^0 beam is coming. Theoretically the range of integration must be from -∞ to x in eq.(15), however, the starting point of integration is limited in practice by spatial coverage of optical system. Therefore error in n_{Li} is greater as x is smaller. Eliminating n_{Li} from eq.(11) by using eq.(15), plasma density is expressed as [5,6,7],

$$n(x) = \frac{I_{Li}(x)\, v_{Li}}{\langle\sigma_{em}v\rangle_{eff} \int_0^x \frac{\langle\sigma_i v\rangle_{eff}}{\langle\sigma_{em}v\rangle_{eff}} I_{Li}(\xi)\, d\xi} \quad \cdots\cdots (16)$$

This method has a great advantage of no need for calibration of beam intensity and optical system as long as the sensitivity of each channel seeing a different position is the same. Since eq.(16) contains effective rate coefficients which are functions of plasma density, the last must be iteratively calculated. Initial profile for iterative calculation is expressed by

$$n(x) = \frac{I_{Li}(x)\, v_{Li}}{\langle\sigma_{is}v\rangle \int_0^x I_{Li}(\xi)\, d\xi}, \quad \cdots\cdots (17)$$

where $\langle\sigma_i v\rangle_{eff}$ and $\langle\sigma_{em}v\rangle_{eff}$ are replaced by the constant value of $\langle\sigma_{is}v\rangle$ and $\langle\sigma_{ex}v\rangle$, respectively. Note that underestimation of ionization rate coefficient in eq.(17) make the approximately reconstructed density greater than the real one. Only several times iterative calculation using eq.(16) can converge the plasma density profile consistently with the obtained emission signal. It has been shown in the practice that the density profile is accurately reconstructed from the edge to the interior of the plasma at the position where the emission signal decreases down to 50~80% of that of the peak[7].

Density profile reconstructed by this method-II is shown in Fig.7. The same emission signal as shown in Fig.6 is employed (thin-dotted curve). Density profile reconstructed by this method-II after ten times iteration is shown in thin-solid curve. The small hump in the profile is not real one. It comes from that data point is discrete and taken in shot by shot base. The result from the method-I is also shown by thick solid curve. Method-II can reconstruct the plasma density beyond the peak position of the emission profile. The

results from the two different methods agree well outside the peak position of the emission signal. Those results are compared with the electron density obtained by ruby laser Thomson scattering, which is shown by a dot with an error bar. Good agreement was obtained although more strict point-to-point correspondence is necessary for the observation points between two diagnostics taking a finite beta shift of the plasma column into account [18].

VI. SELECTION OF DENSITY RECONSTRUCTION METHOD AND EDGE DENSITY PROFILES IN THE CHS

A temporal evolution of plasma density profile in an identical discharge is shown in Fig.8(a) and (b). Vacuum magnetic axis and last closed flux surface are at 94.9cm and 122.5cm, respectively. Plasma is produced by electron cyclotron resonance and heated by neutral beam injection with a duration from 28ms to 128ms of the discharge sequence. The data at 80 ms in the discharge sequence are the same as shown in Fig.6 and 7. Both reconstruction methods are available when the emission signal is attenuated enough in the observation region. In this case reconstruction from the whole region of emission profile (method-II) is applied since the coverage of reconstruction is larger. Density profiles reconstructed by method-II are plotted by solid curves in the both figures. On the other hand, in case that the emission signal is not attenuated enough, only reconstruction from the fractional part of the emission with calibration (method-I) is available. Density profiles reconstructed by method-I are shown in dotted curves in the figures. Coverage of reconstruction is enough wide since peak of emission signal is at a deep position in the plasma. In this way, suitable reconstruction method is selected whether whole emission profile is obtained or not for each datum in Fig.8(a). In Fig.8(b), the method-I or method-II are selected for the region outside or inside the LCFS. By selecting these two types of reconstruction methods, edge plasma density profile in the CHS for various condition of discharge can be obtained. The details of experimental results obtained by this fast Li^0 beam probe system with these density reconstruction algorithms will be discussed in elsewhere [15].

VII. SUMMARY

Two types of density reconstruction methods successfully unfold the edge density profiles in the CHS helical device. Plasma density dependences of ionization and emission

rates are solved by using effective rate coefficients calculated from collisional radiative model. Each method uses the different way to take the effects of beam attenuation into account. The underestimation of ionization rate and overestimation of emission rate, which are caused by neglecting the high density effects of atomic processes, make the reconstructed density smaller than the real one when the reconstruction from the fractional part of emission profile with calibration (method-I) is applied. On the other hand, these mis-estimation can cause larger reconstructed density than the real one when reconstruction from the whole emission profile (method-II) is applied. The plasma density profiles in the edge region for many kinds of discharge are successfully unfolded by choosing one of the available algorithms depending whether the over-all emission profile is obtained or only a part of it is available. The fast Li^0 beam probing system with the new density reconstruction algorithms is established as a powerful tool to investigate edge plasma phenomena in the fusion device.

ACKNOWLEDGMENTS

One of the authors (S.S.) would like to thank Drs. K.N. Sato, T. Kato, M. Fukao and Y. Uesugi for valuable discussions. Other one (M.U.) would like to thank to the partial support of JSPS (Japan) and CNPq (Brazil). Helpful discussions with Dr. K. McCormick as a visiting professor to NIFS are also acknowledged. We also thank Drs. K. Matsuoka, K. Nishimura, H. Yamada and other CHS staffs for continuous help in the experiments. This work has been supported partly by the Grant-in-Aid of Scientific Research from Ministry of Education, Science and Culture.

REFERENCES

[1] A. Pospieszczyk, F Aumayr, H. L. Bay, E. Hintz, P. Leismann, Y. T. Lie, G. G. Ross, D. Rusbüldt, R. P. Schorn, B. Schweer and H. Winter, J. Nucl. Mater. **128&129**,574(1989).

[2] L. Weixelbaum, E. Hayess, U. Wenzel, J. Badalec, K. Jakubka, L.Kryska., J. Stoeckel, M. Valovic and F. Zacek, J. Nucl. Mater. **176&177**,904(1990).

[3] A. Komori, A. Yonesu, S. Nagai, T. Mizuuchi, M. Harada, H. Matsuura, F. Sano, H. Zushi, S. Sudo, M. Nakasuga, Y. Kawai, T. Obiki, Jpn. J. Appl. Phys. **30**,3526(1991).

[4] K. Kadota, A. Pospieszczyk, P. Bogen and E. Hintz, IEEE Trans. Plasma Sci. **PS-12**,262(1984).

[5] A. Pospieszczyk and G.G. Ross, Rev. Sci. Instrum. **59**,605(1988).

[6] S. Sasaki, S. Takamura and K. Kadota, Kakuyugo Kenkyu (in Japanese) **62**,282(1989).

[7] S. Sasaki, S. Takamura, Y. Uesugi, Y. Ohkouchi and K. Kadota, Proc. of IAEA TCM on Research using Small Tokamaks, Hefei, China (IAEA,1991) to be published.

[8] J. S. Bakos, G. Bürger, I. B. Földes, P. E. Giese, P. N. Ignácz, G. Petravich, J. Szigeti and S. Zoletnik, Nucl. Fusion **31**,693(1989).

[9] K. Kadota, K. Tsuchida, Y. Kawasumi, and J. Fujita, Plasma Phys, **20**,1011(1978).

[10] K. Kadota, K. Matsunaga, H. Iguchi, M. Fujiwara, K. Tsuchida and J. Fujita, Jpn. J. Appl. Phys. **21**,L260(1982).

[11] H. Iguchi, K. Kadota, K. Takagi, T. Shoji, M. Hosokawa, M. Fujiwara and K. Ikegami, Rev. Sci. Instrum. **56**,1056(1985).

[12] K. McCormick and ASDEX team, Rev. Sci. Instrum. **56**,1063(1985).

[13] K. Matsuoka, S. Kubo, M. Hosowaka, et. al. , Plasma Physics and Controlled Fusion Research, Nice (IAEA,1989) Vol. II, p.411.

[14] J. Fujita, T. Ozaki, H. Iguchi, K. Kadota, K. Takiyama, M. Ueda and K. McCormick, Proc. of IAEA TCM on Research using Small Tokamaks, Hefei, China (IAEA,1991) to be published.

[15] M. Ueda, H. Iguchi, S. Sasaki, J. Fujita, and CHS group, submitted to J. Nucl. Mater.

[16] F. Aumayr and H.Winter, "Atomic Data Base of Lithium-Beam Activated Plasma Diagnostics" IAP-Report 1/87 March(1987).

[17] T. Nagata, J. Phys. Soc. Japan **48**,2068(1980).

[18] H. Yamada, K. Ida, H. Iguchi, et. al., Nucl. Fusion **32**,25(1992).

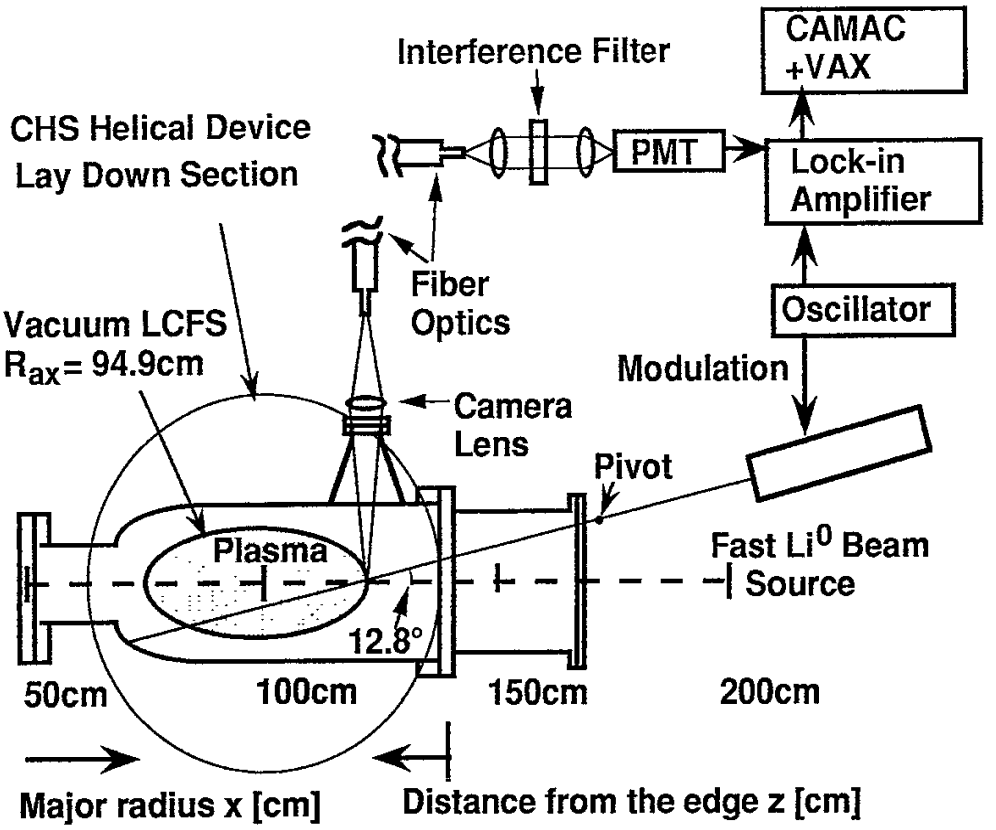

Fig. 1 Experimental setup for fast Li^0 beam probe on CHS.

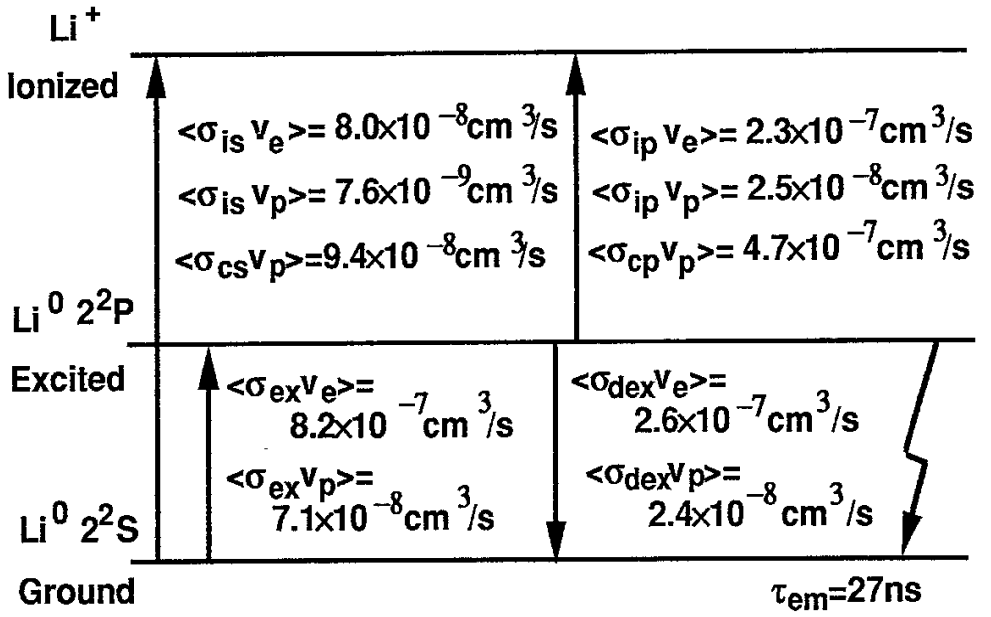

Fig. 2 Atomic processes of Li^0 in the parameter range of CHS edge plasma. Rate coefficients are those at plasma temperature of 30 eV and beam energy of 8 keV.

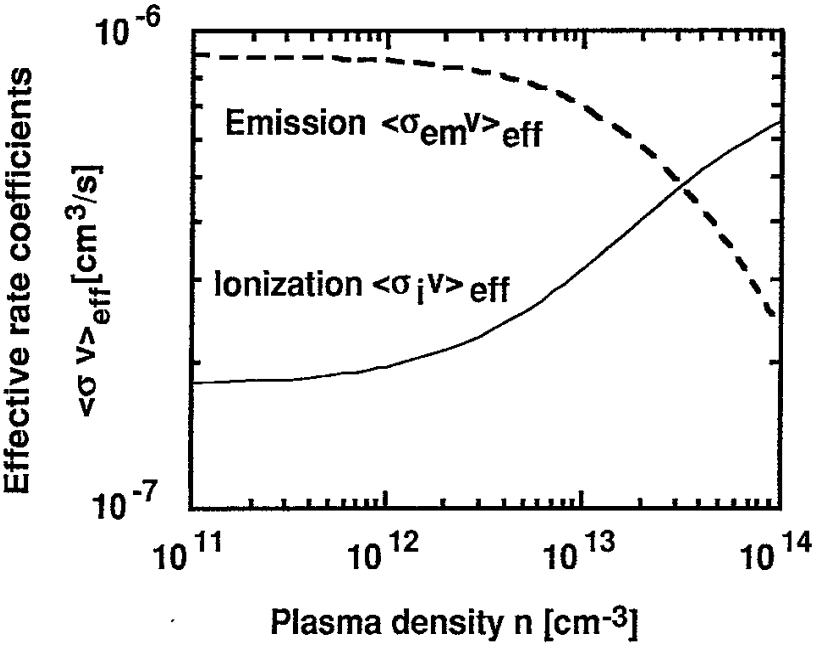

Fig. 3 Density dependence of effective ionization and emission rate coefficients.

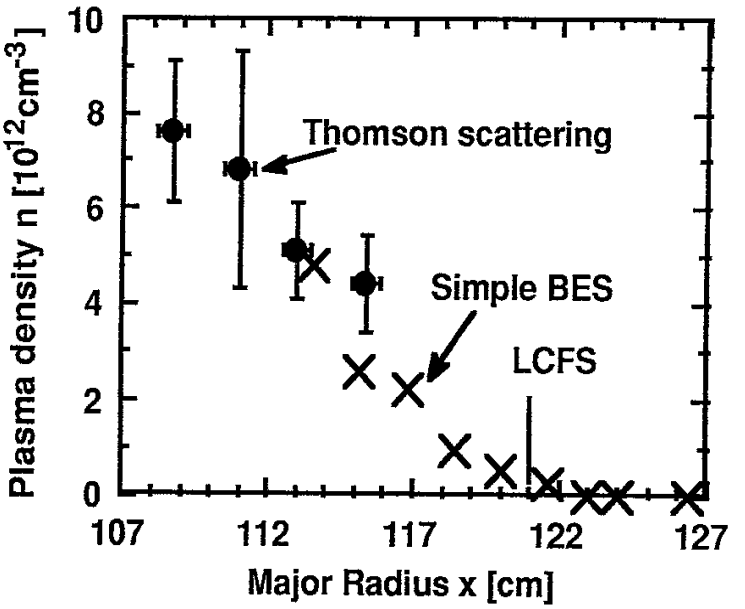

Fig. 4 Result of the density determination by the simple BES measurement for low density discharge as shown by the crosses. Thomson scattering data taken at different toroidal position are also shown by dots with error bars for comparison.

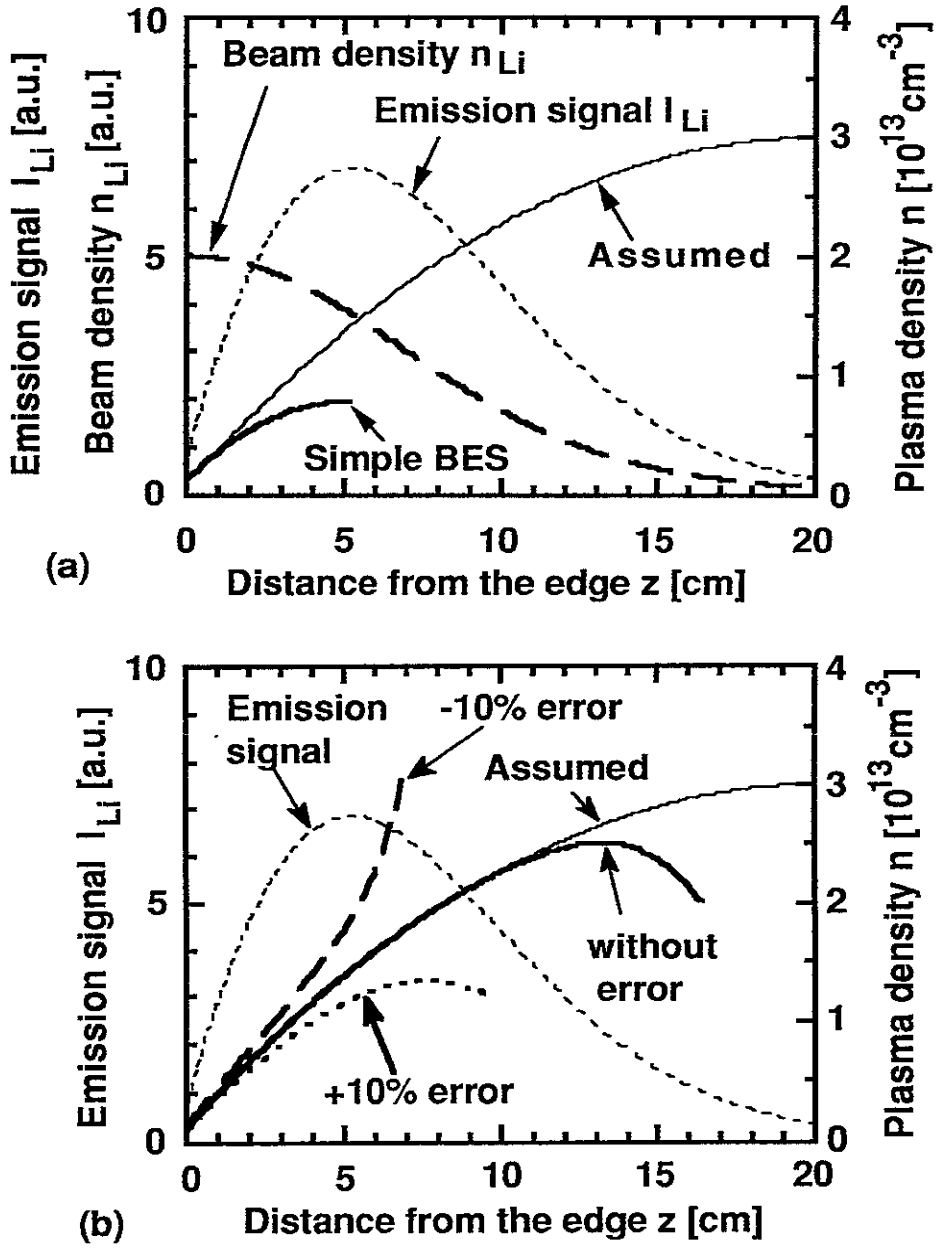

Fig. 5 Numerical simulation of BES with fast Li^0 beam and density reconstruction by method-I for relatively high density plasma. Parabolic distribution of plasma density with the central value of 3×10^{13} cm^{-3} is assumed. (a) Beam density and emission signal are calculated numerically. Simple BES measurement with putting $\langle\sigma_{em}v\rangle_{eff}=\langle\sigma_{ex}v\rangle$ is shown in thick-solid curve. (b) Plasma density reconstructed by method-I from the numerically calculated emission signal. Density reconstruction without calibration error and with +10% and -10% error for w_0 are shown in thick-solid curve, thick-dotted one and thick-dashed one, respectively.

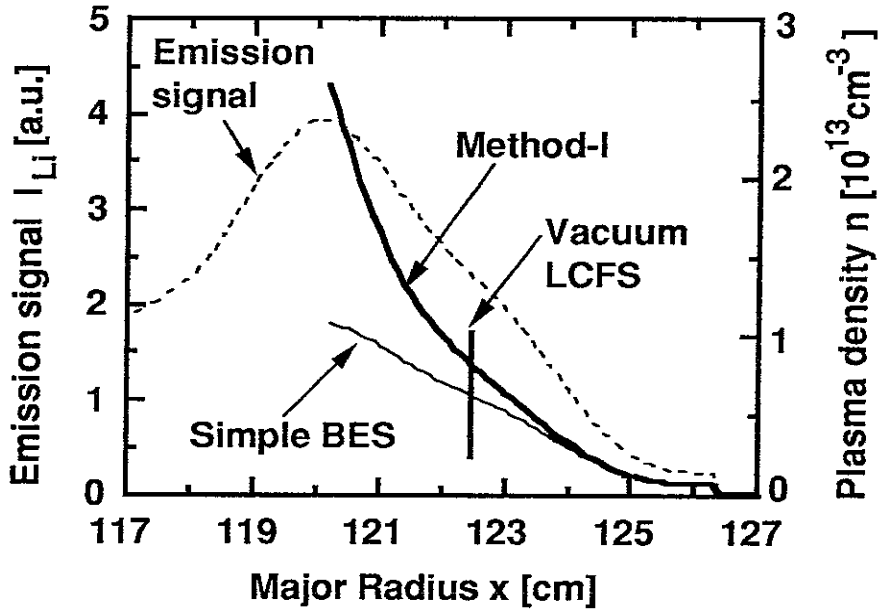

Fig. 6 Result of the density reconstruction by method-I, which is shown in thick-solid curve. Observed emission signal is shown in thin-dotted curve. Simple BES measurement by Eq .(12) with putting $\langle\sigma_{em}v\rangle_{eff}=\langle\sigma_{ex}v\rangle$ is in thin solid one.

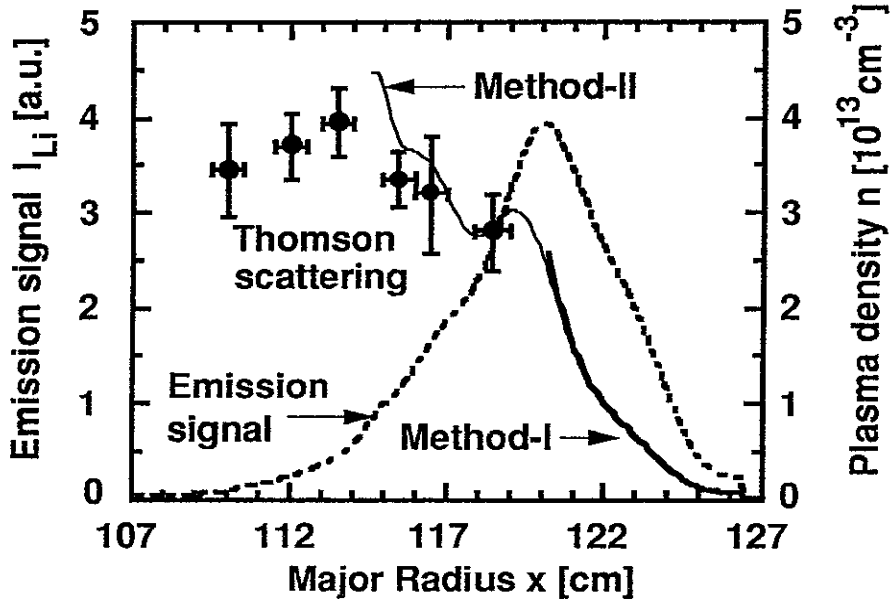

Fig. 7 Results of density reconstruction by method-II, which are shown in thin-solid curves. Emission signal shown in thin dotted curve is the same data as shown in Fig. 6. The result obtained by method-I which is the same datum as shown in Fig. 6 is in thick-solid one. Electron densities obtained by Thomson scattering on the same magnetic flux surface but different toroidal position are plotted by dots with error bars.

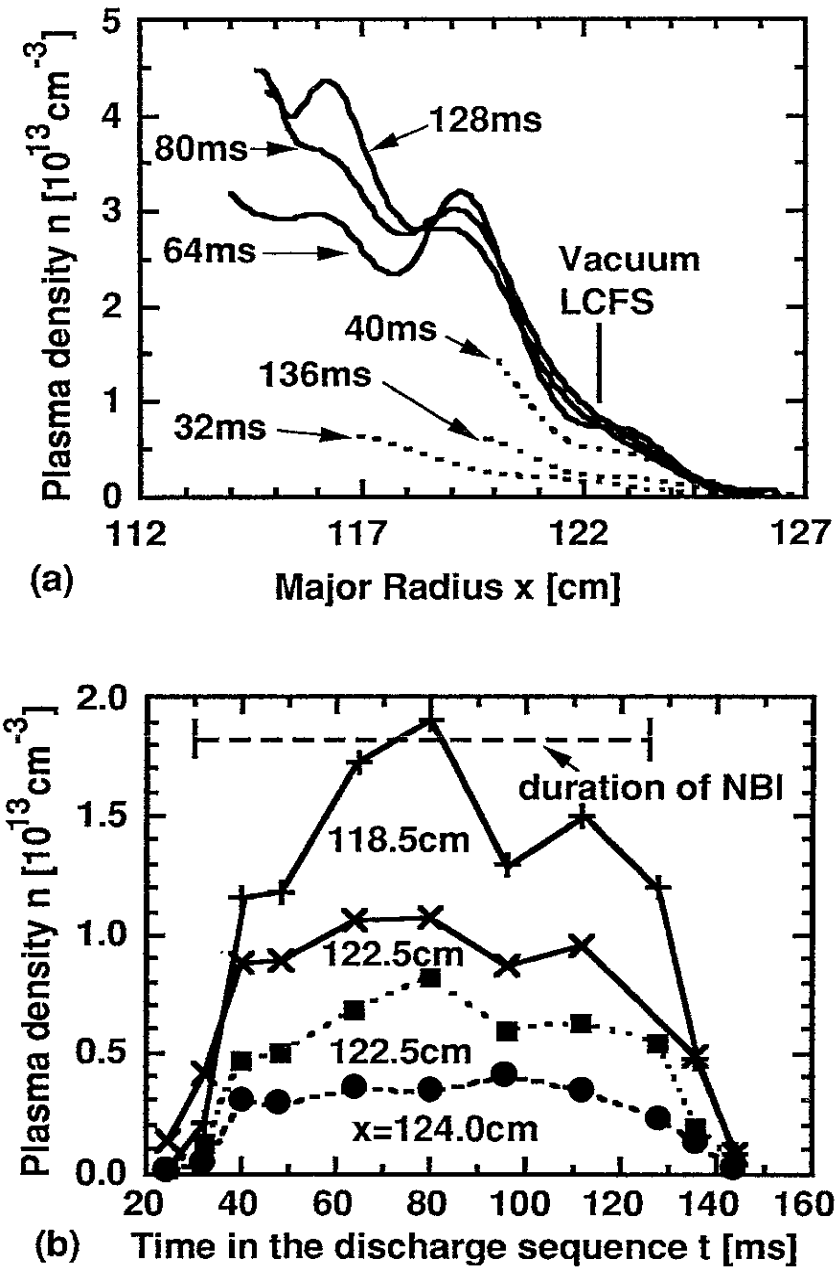

Fig. 8 Temporal evolution of density profile in the CHS discharge. (a) Density profiles reconstructed by method-I and method-II are plotted in dotted and solid curves, respectively. (b) Temporal density change at a fixed position in the discharge sequence. The data outside the LCFS (122.5 cm) plotted by dotted-lines are reconstructed by method-I, and those inside the LCFS plotted by solid-lines are reconstructed by method-II.

Recent Issues of NIFS Series

NIFS-96 S. - I. Itoh, K. Itoh, A. Fukuyama, *ELMy-H mode as Limit Cycle and Chaotic Oscillations in Tokamak Plasmas;* Jun. 1991

NIFS-97 K. Itoh, S. - I. Itoh, H. Sanuki, A. Fukuyama, *An H-mode-Like Bifurcation in Core Plasma of Stellarators;* Jun. 1991

NIFS-98 H. Hojo, T. Watanabe, M. Inutake, M. Ichimura and S. Miyoshi, *Axial Pressure Profile Effects on Flute Interchange Stability in the Tandem Mirror GAMMA 10;* Jun. 1991

NIFS-99 A. Usadi, A. Kageyama, K. Watanabe and T. Sato, *A Global Simulation of the Magnetosphere with a Long Tail : Southward and Northward IMF;* Jun. 1991

NIFS-100 H. Hojo, T. Ogawa and M. Kono, *Fluid Description of Ponderomotive Force Compatible with the Kinetic One in a Warm Plasma* ; July 1991

NIFS-101 H. Momota, A. Ishida, Y. Kohzaki, G. H. Miley, S. Ohi, M. Ohnishi K. Yoshikawa, K. Sato, L. C. Steinhauer, Y. Tomita and M. Tuszewski *Conceptual Design of D-^{3}He FRC Reactor "ARTEMIS"* ; July 1991

NIFS-102 N. Nakajima and M. Okamoto, *Rotations of Bulk Ions and Impurities in Non-Axisymmetric Toroidal Systems* ; July 1991

NIFS-103 A. J. Lichtenberg, K. Itoh, S. - I. Itoh and A. Fukuyama, *The Role of Stochasticity in Sawtooth Oscillation* ; Aug. 1991

NIFS-104 K. Yamazaki and T. Amano, *Plasma Transport Simulation Modeling for Helical Confinement Systems;* Aug. 1991

NIFS-105 T. Sato, T. Hayashi, K. Watanabe, R. Horiuchi, M. Tanaka, N. Sawairi and K. Kusano, *Role of Compressibility on Driven Magnetic Reconnection ;* Aug. 1991

NIFS-106 Qian Wen - Jia, Duan Yun - Bo, Wang Rong - Long and H. Narumi, *Electron Impact Excitation of Positive Ions - Partial Wave Approach in Coulomb - Eikonal Approximation* ; Sep. 1991

NIFS-107 S. Murakami and T. Sato, *Macroscale Particle Simulation of Externally Driven Magnetic Reconnection;* Sep. 1991

NIFS-108 Y. Ogawa, T. Amano, N. Nakajima, Y. Ohyabu, K. Yamazaki, S. P. Hirshman, W. I. van Rij and K. C. Shaing, *Neoclassical*

Transport Analysis in the Banana Regime on Large Helical Device (LHD) with the DKES Code; Sep. 1991

NIFS-109 Y. Kondoh, *Thought Analysis on Relaxation and General Principle to Find Relaxed State;* Sep. 1991

NIFS-110 H. Yamada, K. Ida, H. Iguchi, K. Hanatani, S. Morita, O. Kaneko, H. C. Howe, S. P. Hirshman, D. K. Lee, H. Arimoto, M. Hosokawa, H. Idei, S. Kubo, K. Matsuoka, K. Nishimura, S. Okamura, Y. Takeiri, Y. Takita and C. Takahashi, *Shafranov Shift in Low-Aspect-Ratio Heliotron / Torsatron CHS* ; Sep 1991

NIFS-111 R. Horiuchi, M. Uchida and T. Sato, *Simulation Study of Stepwise Relaxation in a Spheromak Plasma ;* Oct. 1991

NIFS-112 M. Sasao, Y. Okabe, A. Fujisawa, H. Iguchi, J. Fujita, H. Yamaoka and M. Wada, *Development of Negative Heavy Ion Sources for Plasma Potential Measurement* ; Oct. 1991

NIFS-113 S. Kawata and H. Nakashima. *Tritium Content of a DT Pellet in Inertial Confinement Fusion* ; Oct. 1991

NIFS-114 M. Okamoto, N. Nakajima and H. Sugama, *Plasma Parameter Estimations for the Large Helical Device Based on the Gyro-Reduced Bohm Scaling* ; Oct. 1991

NIFS-115 Y. Okabe, *Study of Au^- Production in a Plasma-Sputter Type Negative Ion Source* ; Oct. 1991

NIFS-116 M. Sakamoto, K. N. Sato, Y. Ogawa, K. Kawahata, S. Hirokura, S. Okajima, K. Adati, Y. Hamada, S. Hidekuma, K. Ida, Y. Kawasumi, M. Kojima, K. Masai, S. Morita, H. Takahashi, Y. Taniguchi, K. Toi and T. Tsuzuki, *Fast Cooling Phenomena with Ice Pellet Injection in the JIPP T-IIU Tokamak;* Oct. 1991

NIFS-117 K. Itoh, H. Sanuki and S. -I. Itoh, *Fast Ion Loss and Radial Electric Field in Wendelstein VII-Λ Stellarator*; Oct. 1991

NIFS-118 Y. Kondoh and Y. Hosaka, *Kernel Optimum Nearly-analytical Discretization (KOND) Method Applied to Parabolic Equations <<KOND-P Scheme>>;* Nov. 1991

NIFS-119 T. Yabe and T. Ishikawa, *Two- and Three-Dimensional Simulation Code for Radiation-Hydrodynamics in ICF*; Nov. 1991

NIFS-120 S. Kawata, M. Shiromoto and T. Teramoto, *Density-Carrying Particle Method for Fluid*

; Nov. 1991

NIFS-121 T. Ishikawa, P. Y. Wang, K. Wakui and T. Yabe, *A Method for the High-speed Generation of Random Numbers with Arbitrary Distributions;* Nov. 1991

NIFS-122 K. Yamazaki, H. Kaneko, Y. Taniguchi, O. Motojima and LHD Design *Group, Status of LHD Control System Design ; Dec. 1991*

NIFS-123 Y. Kondoh, *Relaxed State of Energy in Incompressible Fluid and Incompressible MHD Fluid* ; Dec. 1991

NIFS-124 K. Ida, S. Hidekuma, M. Kojima, Y. Miura, S. Tsuji, K. Hoshino, M. Mori, N. Suzuki, T. Yamauchi and JFT-2M Group, *Edge Poloidal Rotation Profiles of H-Mode Plasmas in the JFT-2M Tokamak ;* Dec. 1991

NIFS-125 H. Sugama and M. Wakatani, *Statistical Analysis of Anomalous Transport in Resistive Interchange Turbulence* ;Dec. 1991

NIFS-126 K. Narihara, *A Steady State Tokamak Operation by Use of Magnetic Monopoles* ; Dec. 1991

NIFS-127 K. Itoh, S. -I. Itoh and A. Fukuyama, *Energy Transport in the Steady State Plasma Sustained by DC Helicity Current Drive* ;Jan. 1992

NIFS-128 Y. Hamada, Y. Kawasumi, K. Masai, H. Iguchi, A. Fujisawa, JIPP T-IIU Group and Y. Abe, *New Hight Voltage Parallel Plate Analyzer* ; Jan. 1992

NIFS-129 K. Ida and T. Kato, *Line-Emission Cross Sections for the Charge-exchange Reaction between Fully Stripped Carbon and Atomic Hydrogen in Tokamak Plasma*; Jan. 1992

NIFS-130 T. Hayashi, A. Takei and T. Sato, *Magnetic Surface Breaking in 3D MHD Equilibria of l=2 Heliotron* ; Jan. 1992

NIFS-131 K. Itoh, K. Ichiguchi and S. -I. Itoh, *Beta Limit of Resistive Plasma in Torsatron/Heliotron* ; Feb. 1992

NIFS-132 K. Sato and F. Miyawaki, *Formation of Presheath and Current-Free Double Layer in a Two-Electron-Temperature Plasma* ; Feb. 1992

NIFS-133 T. Maruyama and S. Kawata, *Superposed-Laser Electron Acceleration* Feb. 1992

NIFS-134 Y. Miura, F. Okano, N. Suzuki, M. Mori, K. Hoshino, H. Maeda, T. Takizuka, JFT-2M Group, S.-I. Itoh and K. Itoh, *Rapid Change of*

Hydrogen Neutral Energy Distribution at L/H-Transition in JFT-2M H-mode ; Feb. 1992

NIFS-135 H. Ji, H. Toyama, A. Fujisawa, S. Shinohara and K. Miyamoto *Fluctuation and Edge Current Sustainment in a Reversed-Field-Pinch;* Feb. 1992

NIFS-136 K. Sato and F. Miyawaki, *Heat Flow of a Two-Electron-Temperature Plasma through the Sheath in the Presence of Electron Emission;* Mar. 1992

NIFS-137 T. Hayashi, U. Schwenn and E. Strumberger, *Field Line Diversion Properties of Finite β Helias Equilibria;* Mar. 1992

NIFS-138 T. Yamagishi, *Kinetic Approach to Long Wave Length Modes in Rotating Plasmas*; Mar. 1992

NIFS-139 K. Watanabe, N. Nakajima, M. Okamoto, Y. Nakamura and M. Wakatani, *Three-dimensional MHD Equilibrium in the Presence of Bootstrap Current for Large Helical Device (LHD)*; Mar. 1992

NIFS-140 K. Itoh, S. -I. Itoh and A. Fukuyama, *Theory of Anomalous Transport in Toroidal Helical Plasmas;* Mar. 1992

NIFS-141 Y. Kondoh, *Internal Structures of Self-Organized Relaxed States and Self-Similar Decay Phase;* Mar. 1992

NIFS-142 U. Furukane, K. Sato, K. Takiyama and T. Oda, *Recombining Processes in a Cooling Plasma by Mixing of Initially Heated Gas*; Mar. 1992

NIFS-143 Y. Hamada, K. Masai, Y. Kawasumi, H. Iguchi, A. Fijisawa and JIPP T-IIU Group, *New Method of Error Elimination in Potential Profile Measurement of Tokamak Plasmas by High Voltage Heavy Ion Beam Probes;* Apr. 1992

NIFS-144 N. Ohyabu, N. Noda, Hantao Ji, H. Akao, K. Akaishi, T. Ono, H. Kaneko, T. Kawamura, Y. Kubota, S. Morimoto. A. Sagara, T. Watanabe, K. Yamazaki and O. Motojima, *Helical Divertor in the Large Helical Device;* May 1992

NIFS-145 K. Ohkubo and K. Matsumoto, *Coupling to the Lower Hybrid Waves with the Multijunction Grill*; May 1992

NIFS-146 K. Itoh, S. -I.Itoh, A. Fukuyama, S. Tsuji and Allan J. Lichtenberg, *A Model of Major Disruption in Tokamaks*; May 1992